Physics in Medicine and Biology

IPEM Institute of Physics and Engineering in Medicine

ACCEPTED MANUSCRIPT

Phase-contrast breast CT: the effect of propagation distance

To cite this article before publication: Luca Brombal *et al* 2018 *Phys. Med. Biol.* in press https://doi.org/10.1088/1361-6560/aaf2e1

Note

Phase-contrast breast CT: the effect of propagation distance

Luca Brombal[1,2], Sandro Donato[1,2], Diego Dreossi[3], Fulvia Arfelli[1,2], Deborah Bonazza[4], Adriano Contillo[5,6], Pasquale Delogu[7,8], Vittorio Di Trapani[7,8], Bruno Golosio[9,10], Giovanni Mettivier[11,12], Piernicola Oliva[13,10], Luigi Rigon[1,2], Angelo Taibi[5,6] and Renata Longo[1,2]

[1]Department of Physics, University of Trieste, Via A. Valerio 2, 34127 Trieste, Italy
[2]INFN Division of Trieste, Via A. Valerio 2, 34127 Trieste, Italy
[3]Elettra-Sincrotrone Trieste S.C.p.A, 34149 Basovizza Trieste, Italy
[4]Department of Medical Science, Cattinara Hospital, University of Trieste, Strada di Fiume 447, 34149 Trieste, Italy
[5]Department of Physics and Earth Science, University of Ferrara, Via Savonarola 9, 44121 Ferrara, Italy
[6]INFN Division of Ferrara, via Saragat 1, 44122 Ferrara, Italy
[7]Department of Physical sciences, Earth and Environment, University of Siena, Strada Laterina 8, 53100 Siena, Italy
[8]INFN Division of Pisa, Largo Bruno Pontecorvo 3, 56127 Pisa, Italy
[9]Department of Physics, University of Cagliari, Monserrato-Sestu, I-09042 Monserrato, Italy
[10]INFN Division of Cagliari, Monserrato-Sestu, I-09042 Monserrato, Italy
[11]Department of Physics, University of Napoli Federico II, Via Cinthia, 80126 Fuorigrotta, Napoli, Italy
[12]INFN Division of Napoli, Via Cinthia, 80126 Fuorigrotta, Napoli, Italy
[13]Department of Chemistry and Pharmacy, University of Sassari, Via Vienna, 07100 Sassari SS, Italy

E-mail: luca.brombal@ts.infn.it

July 2018

Abstract. X-ray phase imaging has the potential to dramatically improve soft tissue contrast sensitivity, which is a crucial requirement in many diagnostic applications such as breast imaging. In this context, a program devoted to perform *in-vivo* phase-contrast synchrotron radiation breast computed tomography is ongoing at the Elettra facility (Trieste, Italy). The used phase-contrast technique is the propagation-based configuration, which requires a spatially coherent source and a sufficient object-to-detector distance. In this work the effect of this distance on image quality is quantitatively investigated scanning a large breast surgical specimen at 3 object-to-detector distances (1.6, 3, 9 m) and comparing the images both before and after applying the phase-retrieval procedure. The sample is imaged at 30 keV with a 60 μm pixel pitch CdTe single-photon-counting detector, positioned at a fixed distance of 31.6 m from the source. The detector fluence is kept constant for all acquisitions. The study shows that, at the largest distance, a 20-fold SNR increase can be obtained by

applying the phase-retrieval procedure. Moreover, it is shown that, for phase-retrieved images, changing the object-to-detector distance does not affect spatial resolution while boosting SNR (4-fold increase going from the shortest to the largest distance). The experimental results are supported by a theoretical model proposed by other authors, whose salient results are presented in this paper.

Submitted to: *Phys. Med. Biol.*

1. Introduction

X-ray breast imaging is an extremely demanding task since high contrast sensitivity, high spatial resolution and low delivered dose are required. In this context, x-ray phase-contrast-imaging is a powerful tool to dramatically enhance soft tissues contrast sensitivity without increasing dose. The advantage of phase-contrast imaging over the conventional absorption imaging is based on the fact that, considering soft tissues and energies in the range $10 - 100$ keV, the decrement from unity (δ) of the refraction index (n), responsible for phase effects, is about 3 orders of magnitude higher than the absorption term (β), used in the conventional radiology (Rigon 2014). Several approaches exist to transform the object-induced phase shift into intensity modulations on the detector: interferometric (e.g., gratings), analyzer-based, edge-illumination and free-space-propagarion techniques are in use with synchrotron and, in some cases, conventional sources (Bravin et al. 2012, Rigon 2014). From the experimental point of view, the single-shot free-space propagation-based technique is the easiest to implement since it only requires to increase the object-to-detector distance without using optical elements or multi-exposure acquisition. On the contrary, propagation-based imaging has more stringent requirements on the x-ray source spatial coherence and detector spatial resolution with respect to other techniques (e.g., gratings, edge illumination) (Pfeiffer et al. 2006, Olivo & Speller 2007). Images acquired with the propagation-based technique show an enhanced contrast in the tissue interfaces (i.e., edge-enhancement), which in the ray-optical approximation is proportional to the Laplacian of the object-induced phase-sihft (Peterzol et al. 2005). The edge-enhanced images can be processed by applying a phase-retrieval (PhR) algorithm which allows, under certain approximations, to recover the induced phase-shift (Burvall et al. 2011). In this work the PhR algorithm based on the homogeneous transport of intensity equation proposed by Paganin and co-workers in 2002 is used (Paganin et al. 2002). In fact, the combined effect of free-space propagation and PhR is to increase the image signal-to-noise ratio (SNR) preserving spatial resolution and, far from sharp interfaces where edge-enhancement is present, contrast (Gureyev et al. 2017).

Along with phase effects, breast imaging can also take advantage of 3D techniques, such as breast tomosynthesis and breast CT (BCT), which overcome the superposition of the structures inherent in planar imaging potentially hindering the detection of massive

lesions. At present, the development of BCT systems is a hot topic for several research groups and companies, the main challenge being the trade-off between spatial resolution and delivered dose (Sechopoulos 2013, Sarno et al. 2015, Rößler et al. 2017, Kalender et al. 2017).

In this context, the SYRMA-3D (synchrotron radiation for mammography) collaboration aims to set-up the first clinical study of phase-contrast synchrotron radiation BCT at the Elettra synchrotron facility (Trieste, Italy) and promising results on breast specimens have been recently obtained (Longo et al. 2016, Brombal et al. 2018a, Donato et al. 2018).

In this work, the effect of the propagation distance on the image quality, based on scans of total mastectomy specimen acquired at 3 propagation distances, is discussed. Specifically, both the effects of propagation distance and PhR on image metrics as signal-to-noise-ratio, contrast and spatial resolution are reported and compared with a theoretical model proposed by Gureyev, Nesterets and collaborators (Gureyev et al. 2017, Nesterets & Gureyev 2014), which is briefly described in the next section. A major improvement in signal-to-noise ratio at longer propagation distances and at a constant spatial resolution is experimentally demonstrated.

2. Materials and methods

2.1. Theoretical model

Let us consider an object positioned at a distance R_1 from a monochromatic point x-ray source and at a distance R_2 from a 1D detector (the extension to a 2D detector is straightforward). We further suppose that the incident scalar electromagnetic wave obeys to the homogeneous transport of intensity equation (TIE-hom), so that the intensity at the detector plane ($I_{R_2}(x)$, with x the pixel coordinate) is:

$$I_{R_2}(x) \simeq \left[1 - \sigma^2 \nabla_x^2\right] I_0(x) \quad , \tag{1}$$

$I_0(x)$ being the transmitted intensity in the object plane while $\sigma^2 = \gamma R' \lambda/(4\pi)$ accounts for the (effective) propagation distance $R' = (R_1 R_2)/(R_1 + R_2)$, for the x-ray wavelength λ and for the proportionality factor between the refraction and absorption properties of an interface between 2 materials $\gamma = (\delta_2 - \delta_1)/(\beta_2 - \beta_1)$ (Gureyev et al. 2017). It is worth noticing that, along with its validity conditions, equation 1 implies that the image recorded at a given distance from the object will be similar to the (absorption) contact plane image (i.e., at a null propagation distance) apart from the object's interfaces, where the Laplacian of the intensity is expected to be significantly different from zero. Therefore, within uniform regions of the images (i.e., far from sharp details), neither the detected signal nor the noise are expected to change significantly upon the propagation process. On the contrary, the spatial resolution improves in the free-space propagation. This can be qualitatively understood considering that the (phase) contrast is increased close to sharp interfaces (i.e., where the Laplacian is not negligible), hence the high spatial frequencies are boosted. The quantitative demonstration of the spatial resolution

improvement associated to free-space propagation imaging can be found in (Gureyev et al. 2017). Once the propagation image has been collected, the phase-retrieved image is obtained by inverting the equation 1. In practice, this is accomplished by convolving the image with a low-pass filter which, in the spatial frequency domain (u), can be described as (Brombal et al. 2018a):

$$H(u) = \left[1 + 4\pi^2\sigma^2u^2\right]^{-1} \quad . \tag{2}$$

From the noise reduction perspective, the phase-retrieval filter has nothing special since any low-pass filter would reduce noise enhancing the SNR. Anyway, the peculiarity of the phase-retrieval procedure, applied along with the free-space propagation technique, is that it restores the resolution that would have been observed in the contact plane image while improving the SNR. This means that, once the phase retrieval has been applied, the spatial resolution of the image is the same at all propagation distances, except for magnification effects. In addition, considering flat portions of the image (i.e., far from sharp interfaces), phase retrieval does not modify the image contrast. This can be understood considering that, in practice, phase retrieval acts as a low pass filter, thus not altering the large area contrast of the image (Gureyev et al. 2017, Kitchen et al. 2017). Moreover, the fact that large area contrast is not affected by the phase-retrieval procedure can also be understood from a physical perspective. In fact, in the analytical derivation of the phase-retrieval formula it is assumed that absorption and phase properties are proportional throughout the object, thus, far from interfaces, large area contrast is not expected to vary (Paganin et al. 2002, Burvall et al. 2011).

If both phase-retrieval and tomographic reconstruction process are considered, it can be demonstrated that the SNR gain associated to the application of phase retrieval in the tomographic image is expected to be (Nesterets & Gureyev 2014):

$$SNR_{gain}(A) = \left[(8/3\pi)\frac{A^2}{\ln(A) - 1}\right]^{1/2} \quad , \tag{3}$$

being $A = \sigma^2/(16h'^2)$ a dimensionless parameter accounting for the object composition, irradiation geometry, beam energy (all described by σ) and the detector effective pixel size $h' = h/M$, where h is the physical pixel size and $M = (R_1+R_2)/R_2$ the magnification factor. To obtain this result the detector is assumed to be ideal, i.e., with $MTF = 1$ up to the Nyquist frequency. The equation 3 is the central result of the model and, as a first approximation, it implies that the SNR gain increases almost linearly with the propagation distance and with the inverse of the square of the effective pixel size. Considering realistic parameters in terms of energy (tens of keV), propagation distance (meters) and pixel size (less than 100 μm), the expected SNR gain is between 1 and 2 orders of magnitude with respect to conventional imaging (Kitchen et al. 2017).

2.2. Experimental setup and sample

The images are acquired at the SYRMEP beamline at Elettra (Tromba et al. 2010). The x-ray beam is produced by one storage ring bending magnet and the energy is

selected in the range 8.5 - 40 keV by means of a Si(111) double-crystal monochromator, providing an energy resolution of 0.1%. The beam's cross section at the detector is 220 (horizontal)×4 mm^2 (vertical, Gaussian shape, FWHM) while the source-to-detector distance is kept at 31.6 m for all measurements. Images are collected at 30 keV positioning the sample at 3 different object-to-detector distances, 1.6, 3 and 9 m, respectively. The laminar shape of the beam, along with long object-to-detector distances, allows to work in a scatter-free geometry without the need of anti-scattering grids (Brombal et al. 2018a). To be consistent with the notation of the model presented in the previous section, the propagation distance (R') is defined as the object-to-detector distance scaled by the magnification factor. Given that the magnifications at the 3 sample positions are 1.05, 1.1 and 1.4, the propagation distances will be 1.5, 2.7 and 6.4 m, respectively. It is worth noticing that, especially at high magnifications, the actual finite dimension of the source should be taken into account since it contributes to the overall image blurring, thus reducing the spatial resolution (Gureyev et al. 2008). Anyway, in this work small magnifications (up to 1.4) are used and the detector spatial resolution is similar to the source size (∼100 μm) (SYRMEP 2016), therefore making the source size contribution to the image blurring (as a first approximation) negligible.

Each scan is performed in 40 seconds, collecting the projections over 180 deg with a rotation speed of 4.5 deg sec^{-1}. The dose, expressed as mean glandular dose (MGD), is evaluated by multiplying the air kerma at the patient position (i.e., 1.6 m object-to-detector distance) by a conversion factor accounting for breast size and glandularity, derived from an ad-hoc developed Monte Carlo simulation based on a GEANT4 code (Mettivier et al. 2015, Fedon et al. 2015). In this study, the delivered MGD at the shortest propagation distance was 25 mGy. At larger distances, since the fluence on the detector was kept roughly constant, the delivered dose was slightly increased (∼ 5% higher at 3 m and ∼ 30% higher at 9 m) due to x-ray attenuation in air. In *in-vivo* applications, this issue can easily be overcome by positioning a vacuum pipe between the object and the detector, thus avoiding air attenuation. In addition, as it will be clear in the next section, it can be argued that air attenuation is largely compensated by the SNR increase at larger distances, leaving room for the possibility of a major dose reduction.

The sample is a total breast mastectomy containing an epithelial and stromal sarcomatoid carcinoma. After the formalin fixation and sealing in a vacuum bag, the sample diameter is of about 12 cm. The Directive 2004/23/EC of the European Parliament and of the Council of 31 March 2004 on setting standards of quality and safety for the donation, procurement, testing, processing, preservation, storage and distribution of human tissues were followed.

The images are collected with a CdTe single-photon-counting detector with a 60 μm pixel pitch (Pixirad-8), comprising an array of 8 modules tiling a total surface of 246 × 25 mm^2, operated in dead-time-free mode at a frame rate of 30 Hz (Bellazzini et al. 2013, Delogu et al. 2017). Each scan is constituted by 1200 projections which first undergo an ad-hoc pre-processing procedure (Brombal et al. 2018b) and subsequently are

phase-retrieved ($\gamma = 795$) and reconstructed via a GPU-based filtered back projection with a Shepp-Logan filtering (Brun et al. 2015). The value of the retrieval parameter γ has been extracted from a publicly available database (Taylor 2015) considering a glandular/adipose interface.

2.3. Image analysis

As a first step the SNR of the images prior to the phase retrieval is measured selecting circular ROIs (4000 pixels each) embedded within tumoral tissue, avoiding sharp edges. According to the TIE model (equation 1) SNR should not change significantly varying the propagation distance if no phase-retrieval is applied, being equal to the SNR that would be observed in the contact plane. To compensate for the beam's magnification, SNR is normalized to square root of the effective pixel size $h' = h/M$, where $h = 60$ μm is the physical pixel pitch and M is the magnification. Moreover, to make up for small fluence variations in different acquisitions, SNR is also normalized to the square root of the average number of counts in the detector N, and defined to be:

$$SNR = \frac{\langle I \rangle}{s(I)} \sqrt{\frac{h'_0}{h'}} \sqrt{\frac{N_0}{N}} \quad , \tag{4}$$

where $\langle I \rangle$ is the mean pixel value, $s(I)$ the standard deviation in the ROI, h'_0 and N_0 are the reference pixel size and and number of counts corresponding to the 1.5 m propagation distance acquisition, respectively. The error associated to the SNR is given by the standard deviation of 5 SNR measurements performed in non-overlapping ROIs. SNR is measured also after the application of the phase-retrieval algorithm and a gain factor is defined as:

$$SNR_{gain} = \frac{SNR_{PhR}}{SNR_{noPhR}} \quad . \tag{5}$$

Subsequently, the image contrast is measured selecting ROIs both within tumor (subscript 1) and adipose (subscript 2) regions:

$$C = \frac{\langle I_1 \rangle - \langle I_2 \rangle}{\langle I_2 \rangle} \times 100 \quad . \tag{6}$$

Since phase retrieval is affecting only image noise while free space propagation is affecting spatial resolution, the contrast should not change neither with the application of the phase retrieval, nor varying the propagation distance. As for the SNR, the error associated to the contrast is given by the standard deviation of 5 contrast values measured in non-overlapping ROI pairs.

The spatial resolution is measured in the phase-retrieved images selecting, for each distance, 3 line profiles across a sharp fat/tumor interface produced by a surgical cut. The line profiles are fitted with an erf and the FWHM of its derivative is measured. The spatial resolution is evaluated as the mean value of the 3 FWHMs and the error is estimated to be the maximum fluctuation around the mean value. According to the theory, excluding the effect of the magnification, the spatial resolution after the PhR should not vary by changing the propagation distance since, for each distance, the PhR is

expected to produce the same resolution that would have been measured in the contact plane image. In order to consider only the instrinsic system's spatial resolution, the FWHM is measured in number of pixels instead of an absolute length.

3. Results and discussion

In figure 1 the reconstructed slices at different propagation distances (1.5, 2.7, 6.4 m) without (a-c) and with (d-f) the phase retrieval are reported. With the aim of a visualization allowing a straightforward comparison between images with and without phase retrieval, all the images have been scaled by a normalization factor such that the average value of fibroglandular tissues far from interfaces is 1 while air is 0. Since tissue relaxation occurred and sample repositioning was needed, some morphological changings (e.g., different position of air gaps within the tissue) are observed at different propagation distances. Care was taken to ensure the best match at all distances in the region enclosed by the dashed line of figure 1 (a), where all the measurements are performed. From the images it can be qualitatively noted that, if no PhR is applied, no major variation in signal and noise is observed by varying the propagation distance, except for the sharp interfaces between adipose (dark grey) and tumor or fibroglandular (bright gray) tissue. On the contrary, increasing the propagation distance, the phase-retrieved reconstructions are smoother and no spatial resolution degradation is observed.

The same effect is reported in a finer detail in figure 2, where a zoom on a sharp adipose/tumor interface produced by a surgical cut is displayed. Considering the non-phase retrieved images (a-c) it is clear that the edge-enhancement effect at the interfaces between the two different tissues is amplified at increasing propagation distances, i.e., the high-spatial frequencies are boosted. This can be better visualized in panels (g-i) reporting line profiles (see dashed line in panels (a-c)) of the non-phase-retrieved images at increasing propagation distances. Besides the edge-enhancement effect, clearly visible in panel (i), the profiles show a high level of noise, possibly hampering tissue differentiation. On the other hand, when the PhR is applied (d-f) the edge appearance does not change by varying the propagation distance and the edge-contrast is not longer present. Considering the respective line profiles reported in panels (j-l), a similar edge sharpness is observed at all distances and, when compared with the non-phase-retrieved images profiles, the noise level is significantly lower.

The quantitative results are reported in table 1. As predicted by the theory the SNR, calculated according to equation 4, does not vary significantly with the propagation distance prior to the PhR, while its increase associated with the phase retrieval is greater than a factor of 20 when considering 6.4 m of propagation distance. In addition, it must be noted that only little contrast variations (below 3%) are observed when changing the distance while, at a given position, no significant contrast alterations are associated to the PhR algorithm whose action is limited to image noise. Furthermore, considering phase-retrieved images, the FWHM measured in pixel units does not vary significantly with the propagation distances and, in all cases, was found to be slightly

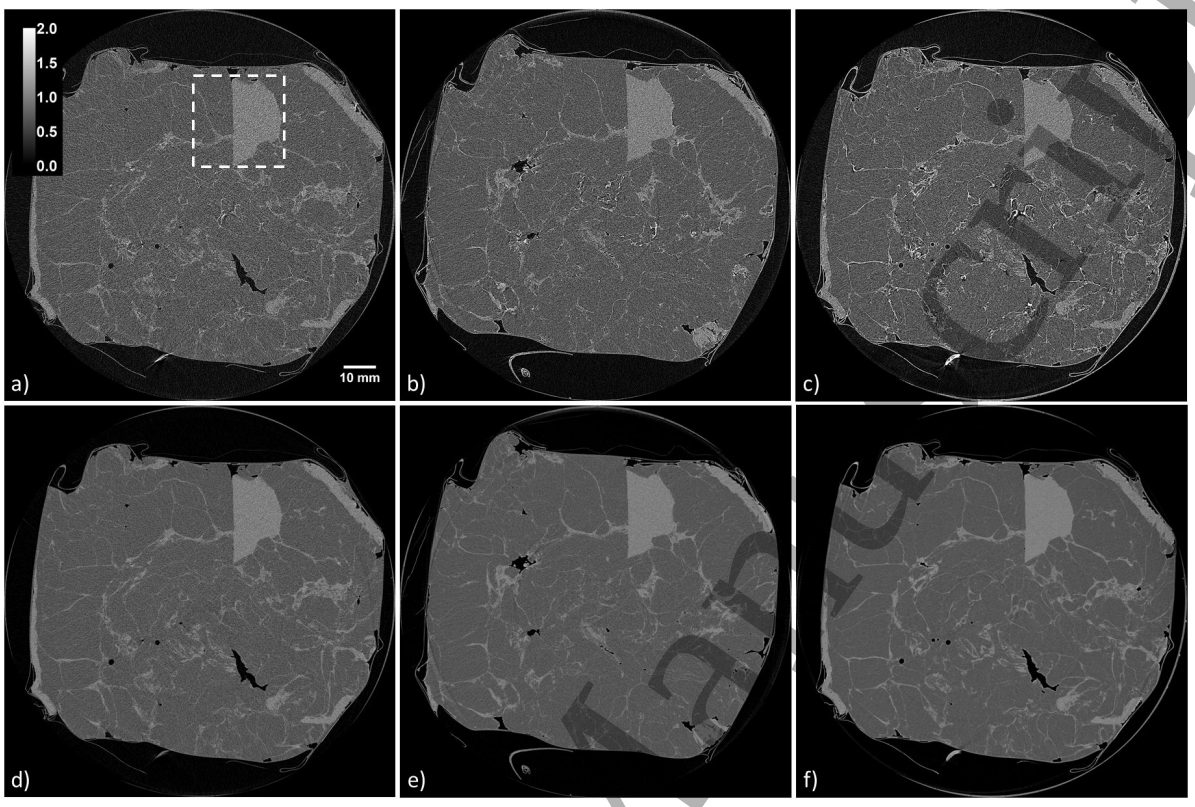

Figure 1. Reconstructed slice acquired at propagation distances 1.5 m (a, d), 2.7 m (b, e) and 6.4 m (c, f). Images in the first row (a-c) are reconstructed without PhR, images in the second row (d-f) with PhR. The dashed square in (a) is the zoom region reported in figure 2. After the normalization described in text, images are displayed in a gray scale window ranging from 0 to 2, where 0 is a typical value of air and 1 a typical value of fibroglandular tissue. Morphological variations at different distances are due to sample repositioning and tissue relaxation within the sample holder.

higher than 2 pixels ($\sim 120\mu$m on the detector plane). This implies that, taking into account the magnification, the actual spatial resolution is improved at longer distances (FWHM $\sim 100\mu$m) at the expense of a smaller field of view.

Table 1. Quantitative results. The uncertainty associated to each measure is enclosed between round brackets.

	PhR	Distance R'		
		1.52 m	2.72 m	6.44 m
SNR	No	1.63 (0.02)	1.63 (0.03)	1.62 (0.01)
	Yes	8.45 (0.13)	13.3 (0.3)	33.8 (0.7)
Contrast	No	32.8 (0.4)	30.6 (0.3)	33.3 (0.2)
	Yes	32.7 (0.2)	30.7 (0.1)	32.9 (< 0.1)
FWHM (px)	Yes	2.1 (0.5)	2.3 (0.3)	2.4 (0.2)

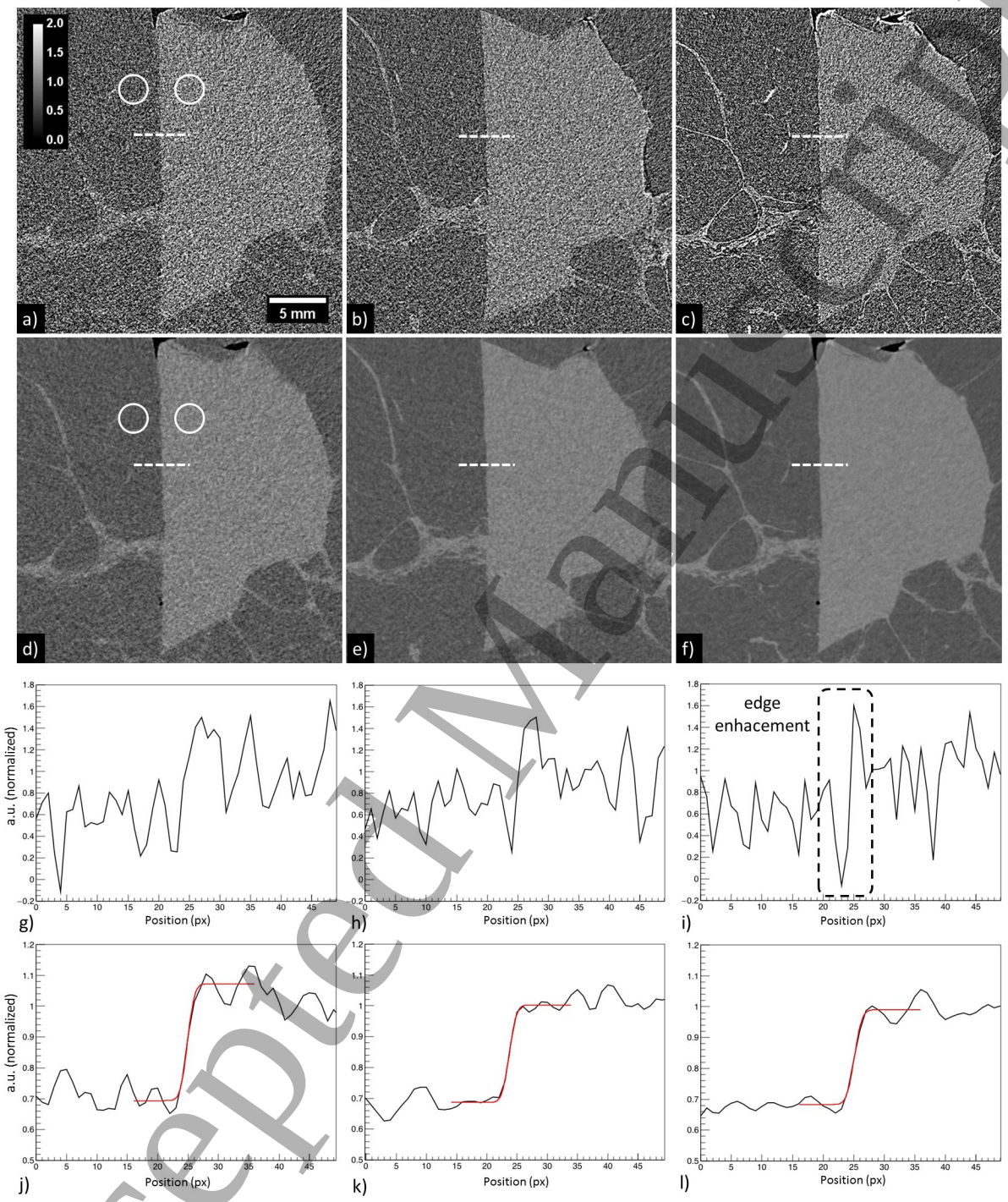

Figure 2. Zoomed detail of figure 1 without (a-c) and with (d-f) phase retrieval at increasing propagation distances (from left to right). In panels (g-i) profiles obtained from the dashed lines in (a-c) are reported. In panels (j-l) profiles obtained from the dashed lines in (d-f) are reported along with the *erf* fit (red curve). In (a) and (d) one of the five pairs of circular ROIs used to determine contrast and SNR are displayed as an example.

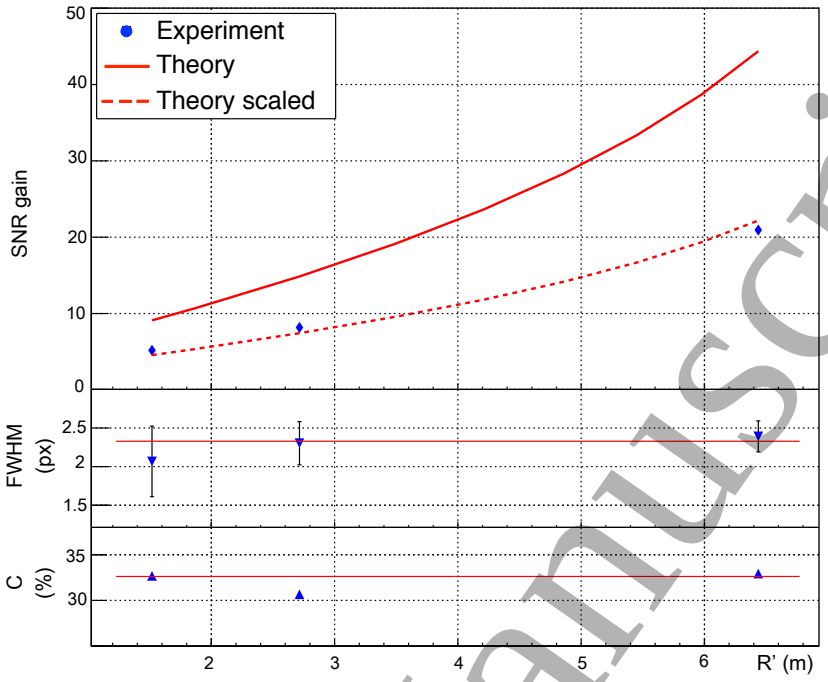

Figure 3. Comparison between experimental results (blue points) and theoretical predictions (solid red lines) as a function of the propagation distance. In the top panel the theoretical prediction scaled by a factor of 2 (dashed red line) is also reported. Some error bars are smaller than points.

With the aim of a better data visualization, the measured SNR gain, contrast and spatial resolution concerning the phase-retrieved images (blue points) and the theoretical predictions (solid red lines) are plotted as a function of the propagation distance in figure 3. From the top panel it can be seen that the measured SNR gain is lower than the predicted value at all propagation distances by roughly a factor of 2. This can be simply explained considering that the model assumes an ideal detector with a constant MTF up to the Nyquist frequency, thus constituting in practice an upper limit for the SNR gain when a real detector is considered. Once the theoretical curve is scaled (dashed red line), the experimental points match the theoretical trend. Moreover, comparing phase-retrieved images, a 4-fold increase in SNR can be obtained at 6.4 m with respect to the shortest propagation distance (1.5 m). At the same time, as predicted by the model, the spatial resolution is kept constant at all the distances (central panel) while only little contrast variations are observed (bottom panel).

4. conclusions

This study on a surgical breast specimen indicates that, combining the free-space propagation phase-contrast technique and the phase-retrieval algorithm, it is possible to obtain a major SNR improvement with respect to conventional imaging, at a constant spatial resolution. Specifically, at a fixed detector fluence, the longer propagation

distances provide higher SNR while leaving spatial resolution unaltered. The maximum observed SNR gain associated with the phase-retrieval algorithm is found to be 20 at 6.4 m while, at all propagation distances, the gain is about a factor of 2 smaller than the one predicted by the presented theoretical model which considers an ideal detector with a constant MTF. This means that the trend of the experimental points is consistent with the theory while the quantitative discrepancies should be attributed to the realistic (non-ideal) detector MTF. For the phase retrieved images, the spatial resolution measured across a sharp adipose/tumoral interface, is slightly higher than $100\mu m$ at all the propagation distances. In addition, it has been shown that, with the described experimental setup, major contrast variations are not observed neither changing propagation distance nor applying the phase-retrieval. This fact is of great importance in sight of the clinical application of this technique, since the image appearance will look "familiar" to the clinician's eye, who will not need a specific training to read the images. The presented work, where one sample was scanned at a limited number of propagation distances, will be expanded using different samples, propagation distances and including the detector's MTF in the theoretical model. Moreover, the SYRMEP beamline is being re-designed to accommodate larger patient-to-detector distances (1.6 m in the present configuration) to better exploit the advantages of the free-space propagation technique in breast CT clinical applications.

Acknowledgments

The authors gratefully thank Timur Gureyev and Yakov Nesterets for the fruitful discussion on the theoretical model and Giuliana Tromba for her support in the experimental activities. The authors gratefully acknowledge all the members of the SYRMA-3D project, Elettra-Sincrotrone Trieste SCpA and the Cattinara University Hospital for their support. Sandro Donato is partially supported by Consorzio per la Fisica Trieste.

References

Bellazzini, R., Spandre, G., Brez, A., Minuti, M., Pinchera, M. & Mozzo, P. (2013). Chromatic x-ray imaging with a fine pitch cdte sensor coupled to a large area photon counting pixel asic, *Journal of Instrumentation* **8**(02): C02028.

Bravin, A., Coan, P. & Suortti, P. (2012). X-ray phase-contrast imaging: from pre-clinical applications towards clinics, *Physics in Medicine & Biology* **58**(1): R1.

Brombal, L., Donato, S., Brun, F., Delogu, P., Fanti, V., Oliva, P., Rigon, L., Di Trapani, V., Longo, R. & Golosio, B. (2018b). Large-area single-photon-counting cdte detector for synchrotron radiation computed tomography: a dedicated pre-processing procedure, *Journal of Synchrotron Radiation* **25**(4).

Brombal, L., Golosio, B., Arfelli, F., Bonazza, D., Contillo, A., Delogu, P., Donato, S., Mettivier, G., Oliva, P., Rigon, L. et al. (2018a). Monochromatic breast ct: absorption and phase-retrieved images, *Medical Imaging 2018: Physics of Medical Imaging*, Vol. 10573, International Society for Optics and Photonics, p. 1057320.

Brun, F., Pacilè, S., Accardo, A., Kourousias, G., Dreossi, D., Mancini, L., Tromba, G. & Pugliese, R. (2015). Enhanced and flexible software tools for x-ray computed tomography at the italian synchrotron radiation facility elettra, *Fundamenta Informaticae* **141**(2-3): 233–243.

Burvall, A., Lundström, U., Takman, P. A., Larsson, D. H. & Hertz, H. M. (2011). Phase retrieval in x-ray phase-contrast imaging suitable for tomography, *Optics express* **19**(11): 10359–10376.

Delogu, P., Golosio, B., Fedon, C., Arfelli, F., Bellazzini, R., Brez, A., Brun, F., Di Lillo, F., Dreossi, D., Mettivier, G. et al. (2017). Imaging study of a phase-sensitive breast-ct system in continuous acquisition mode, *Journal of Instrumentation* **12**(01): C01016.

Donato, S., Brombal, L., Tromba, G., Longo, R. et al. (2018). Phase-contrast breast-ct: Optimization of experimental parameters and reconstruction algorithms, *World Congress on Medical Physics and Biomedical Engineering 2018, IFMBE Proceedings*, Vol. 61, Springer, pp. 109–115.

Fedon, C., Longo, F., Mettivier, G. & Longo, R. (2015). Geant4 for breast dosimetry: parameters optimization study, *Physics in Medicine & Biology* **60**(16): N311.

Gureyev, T. E., Nesterets, Y. I., Kozlov, A., Paganin, D. M. & Quiney, H. M. (2017). On the unreasonable effectiveness of transport of intensity imaging and optical deconvolution, *JOSA A* **34**(12): 2251–2260.

Gureyev, T. E., Nesterets, Y. I., Stevenson, A. W., Miller, P. R., Pogany, A. & Wilkins, S. W. (2008). Some simple rules for contrast, signal-to-noise and resolution in in-line x-ray phase-contrast imaging, *Optics express* **16**(5): 3223–3241.

Kalender, W. A., Kolditz, D., Steiding, C., Ruth, V., Lück, F., Rößler, A.-C. & Wenkel, E. (2017). Technical feasibility proof for high-resolution low-dose photon-counting ct of the breast, *European radiology* **27**(3): 1081–1086.

Kitchen, M. J., Buckley, G. A., Gureyev, T. E., Wallace, M. J., Andres-Thio, N., Uesugi, K., Yagi, N. & Hooper, S. B. (2017). Ct dose reduction factors in the thousands using x-ray phase contrast, *Scientific reports* **7**(1): 15953.

Longo, R., Arfelli, F., Bellazzini, R., Bottigli, U., Brez, A., Brun, F., Brunetti, A., Delogu, P., Di Lillo, F., Dreossi, D. et al. (2016). Towards breast tomography with synchrotron radiation at elettra: first images, *Physics in Medicine & Biology* **61**(4): 1634.

Mettivier, G., Fedon, C., Di Lillo, F., Longo, R., Sarno, A., Tromba, G. & Russo, P. (2015). Glandular dose in breast computed tomography with synchrotron radiation, *Physics in Medicine & Biology* **61**(2): 569.

Nesterets, Y. I. & Gureyev, T. E. (2014). Noise propagation in x-ray phase-contrast imaging and computed tomography, *Journal of Physics D: Applied Physics* **47**(10): 105402.

Olivo, A. & Speller, R. (2007). A coded-aperture technique allowing x-ray phase contrast imaging with conventional sources, *Applied Physics Letters* **91**(7): 074106.

Paganin, D., Mayo, S., Gureyev, T. E., Miller, P. R. & Wilkins, S. W. (2002). Simultaneous phase and amplitude extraction from a single defocused image of a homogeneous object, *Journal of microscopy* **206**(1): 33–40.

Peterzol, A., Olivo, A., Rigon, L., Pani, S. & Dreossi, D. (2005). The effects of the imaging system on the validity limits of the ray-optical approach to phase contrast imaging, *Medical physics* **32**(12): 3617–3627.

Pfeiffer, F., Weitkamp, T., Bunk, O. & David, C. (2006). Phase retrieval and differential phase-contrast imaging with low-brilliance x-ray sources, *Nature physics* **2**(4): 258.

Rigon, L. (2014). x-ray imaging with coherent sources, *Comprehensive Biomedical Physics* **2**: 193–216.

Rößler, A.-C., Kalender, W., Kolditz, D., Steiding, C., Ruth, V., Preuss, C., Peter, S. C., Brehm, B., Hammon, M., Schulz-Wendtland, R. et al. (2017). Performance of photon-counting breast computed tomography, digital mammography, and digital breast tomosynthesis in evaluating breast specimens, *Academic radiology* **24**(2): 184–190.

Sarno, A., Mettivier, G. & Russo, P. (2015). Dedicated breast computed tomography: basic aspects, *Medical physics* **42**(6Part1): 2786–2804.

Sechopoulos, I. (2013). A review of breast tomosynthesis. part i. the image acquisition process, *Medical*

physics **40**(1).

SYRMEP (2016). SYRMEP specifications.
URL: *www.elettra.trieste.it/lightsources/elettra/elettra-beamlines/syrmep/specification.html*

Taylor, J. A. (2015). CSIRO TS imaging.
URL: *www.ts-imaging.net/Services/Simple/ICUtilXdata.aspx*

Tromba, G., Longo, R., Abrami, A., Arfelli, F., Astolfo, A., Bregant, P., Brun, F., Casarin, K., Chenda, V., Dreossi, D. et al. (2010). The syrmep beamline of elettra: Clinical mammography and biomedical applications, *AIP Conference Proceedings*, Vol. 1266, AIP, pp. 18–23.